Simultaneous near-field and far-field fluorescence microscopy of single molecules

Ruckstuhl, Thomas ; Verdes, Daniel ; Winterflood, Christian M ; Seeger, Stefan

Abstract: A new microscope objective is presented for the parallel fluorescence detection below and above the critical angle of total internal reflection with single molecule sensitivity. The collection of supercritical angle fluorescence (SAF) leads to a strongly surface confined detection volume whereas the collection of undercritical angle fluorescence (UAF) allows for the observation of deeper axial sections of the specimen. By simultaneous detection of the near-field-mediated SAF and the far-field UAF emission modes the z-position of emitters can be obtained on the nanometer scale. We investigate the point spread function of the optics and demonstrate nanoscopic z-localization of single molecules. The oil immersion objective, developed for use on common microscope bodies, opens up new possibilities for the study of topographies and dynamics at surfaces and on membranes.

DOI: https://doi.org/10.1364/OE.19.006836

Simultaneous near-field and far-field fluorescence microscopy of single molecules

Thomas Ruckstuhl, Dorinel Verdes, Christian M. Winterflood, and Stefan Seeger*

Institute of Physical Chemistry, University of Zurich, Winterthurerstrasse 190, CH-8057 Zurich, Switzerland
**sseeger@pci.uzh.ch*

Abstract: A new microscope objective is presented for the parallel fluorescence detection below and above the critical angle of total internal reflection with single molecule sensitivity. The collection of supercritical angle fluorescence (SAF) leads to a strongly surface confined detection volume whereas the collection of undercritical angle fluorescence (UAF) allows for the observation of deeper axial sections of the specimen. By simultaneous detection of the near-field-mediated SAF and the far-field UAF emission modes the z-position of emitters can be obtained on the nanometer scale. We investigate the point spread function of the optics and demonstrate nanoscopic z-localization of single molecules. The oil immersion objective, developed for use on common microscope bodies, opens up new possibilities for the study of topographies and dynamics at surfaces and on membranes.

OCIS codes: (180.2520) Fluorescence Microscopy; (180.4243) Near-field microscopy; (080.3620) Lens system design.

References and links

1. E. H. Synge, "A suggested method for extending the microscopic resolution into the ultramicroscopic region," Philos. Mag. **6**, 356–362 (1928).
2. D. W. Pohl, W. Denk, and M. Lanz, "Optical Stethoscopy: Image Recording with Resolution λ/20," Appl. Phys. Lett. **44**(7), 651–653 (1984).
3. A. Lewis, M. Isaacson, A. Harootunian, and A. Muray, "Development of a 500 Å spatial resolution light microscope: I. light is efficiently transmitted through λ/16 diameter apertures," Ultramicroscopy **13**(3), 227–231 (1984).
4. T. Hirschfeld, "Total reflection fluorescence," Can. Spectrosc. **10**, 128 (1965).
5. D. Axelrod, "Cell-substrate contacts illuminated by total internal reflection fluorescence," J. Cell Biol. **89**(1), 141–145 (1981).
6. H. Schneckenburger, "Total internal reflection fluorescence microscopy: technical innovations and novel applications," Curr. Opin. Biotechnol. **16**(1), 13–18 (2005).
7. W. Lukosz, and R. E. Kunz, "Light emission by magnetic and electric dipoles close to a plane interface. I. Total radiated power," J. Opt. Soc. Am. A **67**(12), 1607–1625 (1977).
8. E. D. Hellen, and D. Axelrod, "Fluorescence emission at dielectric and metal-film interfaces," J. Opt. Soc. Am. B **4**(3), 337–350 (1987).
9. J. Enderlein, T. Ruckstuhl, and S. Seeger, "Highly efficient optical detection of surface-generated fluorescence," Appl. Opt. **38**(4), 724–732 (1999).
10. T. Ruckstuhl, J. Enderlein, S. Jung, and S. Seeger, "Forbidden light detection from single molecules," Anal. Chem. **72**(9), 2117–2123 (2000).
11. T. Ruckstuhl, and D. Verdes, "Supercritical angle fluorescence (SAF) microscopy," Opt. Express **12**(18), 4246–4254 (2004).
12. D. Verdes, T. Ruckstuhl, and S. Seeger, "Parallel two-channel near- and far-field fluorescence microscopy," J. Biomed. Opt. **12**(3), 034012 (2007).
13. J. Ries, T. Ruckstuhl, D. Verdes, and P. Schwille, "Supercritical angle fluorescence correlation spectroscopy," Biophys. J. **94**(1), 221–229 (2008).
14. T. Ruckstuhl, and S. Seeger, "Attoliter detection volumes by confocal total-internal-reflection fluorescence microscopy," Opt. Lett. **29**(6), 569–571 (2004).
15. K. Hassler, M. Leutenegger, P. Rigler, R. Rao, R. Rigler, M. Gösch, and T. Lasser, "Total internal reflection fluorescence correlation spectroscopy (TIR-FCS) with low background and high count-rate per molecule," Opt. Express **13**(19), 7415–7423 (2005).
16. N. L. Thompson, and B. L. Steele, "Total internal reflection with fluorescence correlation spectroscopy," Nat. Protoc. **2**(4), 878–890 (2007).

#142685 - $15.00 USD Received 14 Feb 2011; revised 15 Mar 2011; accepted 16 Mar 2011; published 24 Mar 2011

17. C. M. Winterflood, T. Ruckstuhl, D. Verdes, and S. Seeger, "Nanometer axial resolution by three-dimensional supercritical angle fluorescence microscopy," Phys. Rev. Lett. **105**(10), 108103 (2010).
18. B. Richards, and E. Wolf, "Electromagnetic diffraction in optical systems. 2. Structure of the image field in an aplanatic system," Proc. R. Soc. Lond. A **253**(1274), 358–379 (1959).

1. Introduction

The original idea behind near-field optical microscopy was to break Abbe's diffraction barrier by scanning the specimen with a light source of sub-wavelength extension [1]. Near-field scanning optical microscopy has been accomplished using tapered optical fibers with apertures of 100 nm diameter and less [2,3]. Light is not transmitted through apertures far below the wavelength but produces a so-called evanescent wave behind it. The near-field standing wave decays rapidly with the distance to the aperture and allows resolving structures on the scale of nanometers.

Optical near fields can be used to spatially confine observation volumes even without probe tips. In total internal reflection fluorescence (TIRF) microscopy the coverslip surface is illuminated above the critical angle and the resulting evanescent wave above the glass is used to selectively excite the surface-near region of the specimen [4]. This near-field technique is very popular in biology as it enables clear imaging, virtually free of blurred background from regions outside the surface plane [5,6].

Independent from the mode of excitation, any radiating electrical dipole, such as a fluorescing molecule, generates an optical near field. As only the far-field emission propagates into space, the near field usually transmits no energy and remains hidden for a remote detector. However, when the emitter is in proximity to an optical boundary, such as a water/glass interface, the perturbation of the near field leads to the creation of detectable propagating waves. As shown in Fig. 1 the discontinuity of the refractive index within the realm of the near field results in far-field radiation into the glass above the critical angle, θ_c [7–9]. For emitters located directly at a water/glass interface the supercritical angle fluorescence (SAF) accounts for more than one third of the overall emission. The coupling of the near field is exponentially dependent on the distance to the glass and at an emitter-surface distance of only one wavelength the SAF intensity accounts for less than one percent of the overall emission. Consequently, the exclusive collection of SAF can be used to obtain a surface-confined observation volume.

A solid parabolic element has been introduced for the collimation of SAF into a bundle of conveniently processible parallel rays [9]. A practical advantage of this approach is that the lowest collected angle lies at the outer margin of the collimated beam. By means of a circular aperture it is straightforward to set the low limit of collected angles to the desired value above the critical angle. The high collection efficiency of this approach has been demonstrated by the detection of single molecules [10].

In SAF microscopy, the specimen is excited at moderate surface angles, below the critical angle. In this way the excitation beam can be focused to a tight spot of Gaussian intensity profile at the surface [11,12], which is ideal for surface-confined fluorescence correlation spectroscopy (FCS) [13]. In total internal reflection fluorescence correlation spectroscopy (TIRFCS) the constraint of supercritical illumination has prevented the excitation of a laterally confined surface area [14–16]. In SAF microscopy the excitation light is incident below θ_c and penetrates the specimen. Therefore it is possible to visualize deeper axial sections in parallel by separate collection of the far-field emission sent into the angular regime below θ_c into the glass, referred to as undercritical angle fluorescence (UAF).

#142685 - $15.00 USD Received 14 Feb 2011; revised 15 Mar 2011; accepted 16 Mar 2011; published 24 Mar 2011

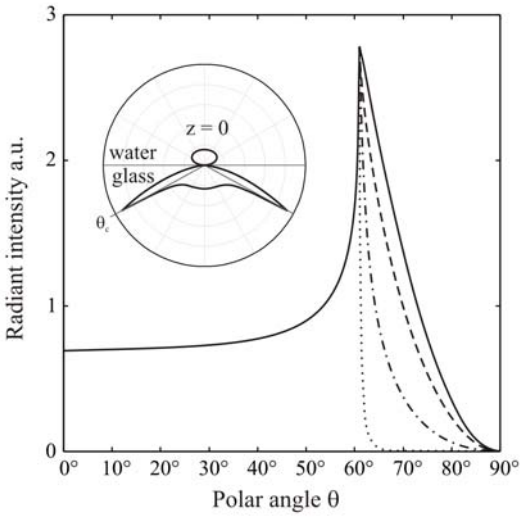

Fig. 1. Angular distribution of the radiant intensity of isotropically oriented dipole emitters into the glass halfspace. The plots were calculated for emitters in water with a distance to the glass surface of z = 0 (solid), z = λ/20 (dashed), z = λ/5 (dash-dotted) and of z = λ (dotted), with the emission wavelength λ. The inset shows a polar plot of the radiant intensity into the entire space for emitters with z = 0. SAF is the proportion of the fluorescence emitted above 61°, the critical angle of the water/glass interface.

The SAF intensity provides an extremely sensitive measure of an emitter's z-position due to its rapid decay along the z-axis. The UAF intensity is barely influenced by an emitter's z-position within the first wavelength above the coverslip and serves as a robust measure for an emitter's intrinsic brightness. We have demonstrated that the simultaneous measurement of both intensities can be used to determine the axial position of fluorescence emitters with nanometer accuracy [17].

Here, we introduce a microscope objective for the straightforward implementation of parallel near-field and far-field microscopy on common microscope bodies. The element provides single molecule detection capacity for both emission modes of SAF and UAF. The properties of the microscope objective are investigated by point spread function (PSF) measurements and by the nanoscopic z-localization of nanospheres and single molecules.

2. Microscope objective design

The oil immersion microscope objective, shown in Fig. 2, is designed for use with conventional glass coverslips of 0.17 mm thickness. It comprises an inner custom-built lens system of 1.0 numerical aperture and a parabolic collector. The inner lens assembly has a clear aperture diameter of 5.3 mm and an effective focal length of 2.8 mm. The infinity corrected optics consists of AR-coated glass lenses and is designed to focus a collimated excitation beam at the coverslip surface. By aberration balancing for the design wavelengths of 514 nm, 532 nm and 635 nm the optics features a diffraction-limited performance over a wide range of the visible spectrum. The inner optics collects UAF up to surface angles of 41° resulting in a fluorescence collection efficiency of 17% for fluorophores in aqueous solution. The inner lens system can also be used for widefield imaging within a diffraction limited field of view of 30 μm diameter. The inner assembly was centered with the optical axis of the outer parabolic collector by means of interferometry. The collector was diamond turned from Zeonex, a polyolefin co-polymer. The outer parabolic element captures the fluorescence emitted at large surface angles between 60° and 80°.

#142685 - $15.00 USD Received 14 Feb 2011; revised 15 Mar 2011; accepted 16 Mar 2011; published 24 Mar 2011

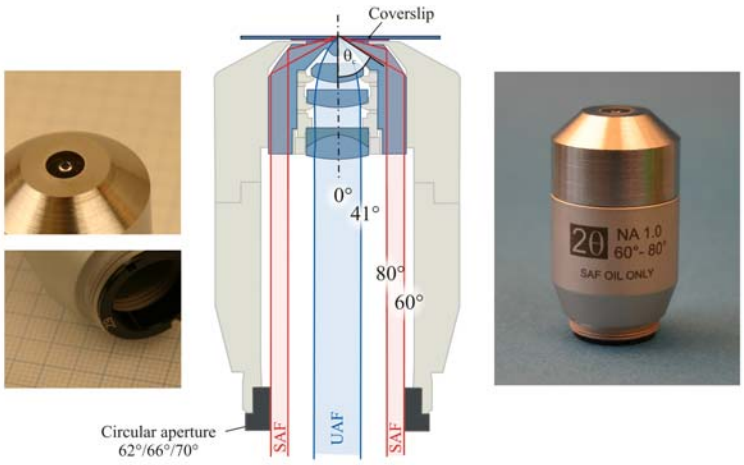

Fig. 2. Photographs and schematic of the developed microscope objective. Due to the reflection at the parabola the lowest collected angle comes to lie at the outside of the ejected annular ring of fluorescence and can be increased straightforwardly by means of a circular aperture.

To obtain a surface-confined detection volume the fluorescence collection needs to be restricted to the angular region above the critical angle, θ_c, given by Snell's law according to

$$\theta_c = \arcsin\left(\frac{n_1}{n_2}\right), \tag{1}$$

where n_1 and n_2 are the refractive indexes of the specimen and the glass, respectively. With n_2 = 1.523 for glass coverslips with low dispersion (Abbe number: 55), the value of θ_c is predominately influenced by the refractive index of the sample. For aqueous samples (n_1 = 1.333) the critical angle is with θ_c = 61° significantly lower than for biological cells (n_1 = 1.38) with θ_c = 65°.

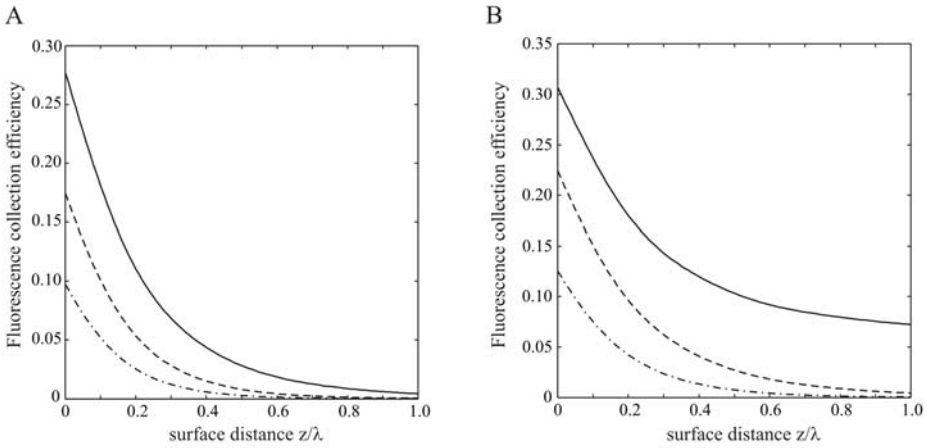

Fig. 3. Z-dependent fluorescence collection efficiency of the outer collector calculated for the angular cut-off at 62° (solid), 66° (dashed) and 70° (dash-dotted) for (A) aqueous solution (n_1 = 1.333, θ_c = 61°) and for (B) a biological cell (n_1 = 1.38, θ_c = 65°). A cut-off angle below the critical angle leads to a loss of the axial confinement of the detection volume. An isotropic dipole orientation was assumed for the calculations of the collection efficiencies.

#142685 - $15.00 USD Received 14 Feb 2011; revised 15 Mar 2011; accepted 16 Mar 2011; published 24 Mar 2011

To ensure the exclusive collection of SAF for different samples an exchangeable circular aperture in the objective housing serves to set the lowest collected angle to 62°, 66° or 70°. The choice of an adequate cut-off angle depends on the angular distribution of radiation, which exhibits a pronounced maximum in direction of the critical angle. As shown in Fig. 3, the exclusion of a wide range of supercritical angles leads to a reduction of the fluorescence collection efficiency and the cut-off angle should be set near θ_c.

3. Microscope composition and alignment

The microscope objective was mounted on the inverted microscope platform IX71 (Olympus, Japan). The right side port of the microscope body provided free optical access (no tube lens in the optical path). Figure 4 shows a schematic of the optical setup. In brief, the beam of a HeNe laser (632.8 nm, 5 mW) was circularly polarized by means of a quarter wave plate and expanded to a beam waist of about 5 mm. An iris was used to avoid that excitation light can enter the parabolic collector of the objective from below. A dichroic beamsplitter located approximately 15 cm in front of the side port separated the excitation and detection beams. In the detection path, a lens (f_1 = 200 mm) positioned 400 mm behind the objective produced an image of the objective's output another 400 mm behind it. There, a lens (f_2 = 200 mm) collimated the beams of SAF and UAF. A 45° rod mirror fixed on a glass window reflected UAF and allowed SAF to pass through. The signals were focused onto the active areas (diameter: 0.18 mm) of identical single photon avalanche diodes (SPADs, PerkinElmer, USA) positioned in the respective image planes. Photon counting was performed with a FIFO buffered PCI-board (6602, National Instruments, USA). Spectral filters were employed in the excitation (BrightLine HC 632/22, Semrock, USA) and the detection path (BrightLine HC 676/29, Semrock). A motorized microscope stage (ScanIm 120 × 100, Märzhäuser, GER) was used for sample scanning.

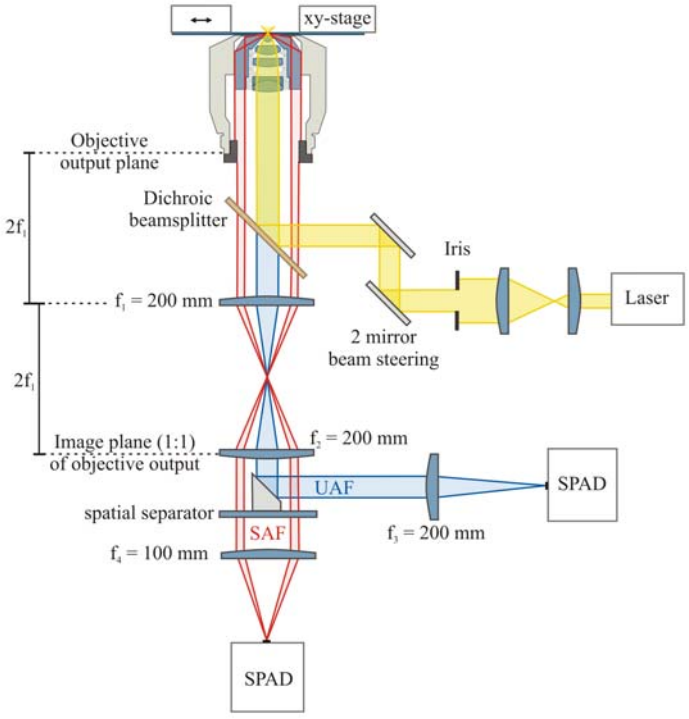

Fig. 4. Schematic of the optical setup.

#142685 - $15.00 USD Received 14 Feb 2011; revised 15 Mar 2011; accepted 16 Mar 2011; published 24 Mar 2011

For the alignment of the microscope, the laser focus was directed across the surface of a coverslip towards the geometrical focus of the objective's parabolic collector by means of two mirror beam steering. This procedure was done using a fluorescence coated coverslip and a camera CCD positioned in detection path. With the laser focus in the designated position SAF is refocused to a small spot in the image plane. Figure 5 shows the intensity distributions of SAF and UAF in the respective image planes.

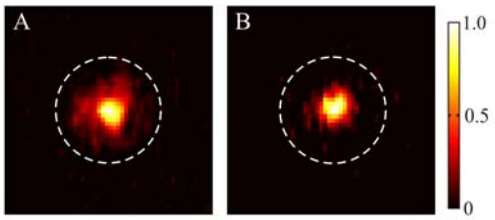

Fig. 5. Intensity distributions measured in the respective image planes of (A) SAF and (B) UAF. The circles indicate the 0.18 mm active area diameter of the SPADs.

4. Point spread function

The lateral PSF of the microscope was measured using red fluorescent beads of 36 nm diameter immobilized on a coverslip below water. The 62° cut-off aperture was used for the SAF collection. Figure 6A shows the UAF image of a bead obtained by sample scanning. The measured UAF-PSF is in excellent agreement with the intensity pattern calculated for a diffraction limited aplanatic optics of 1.0 numerical aperture according to [18] shown in Fig. 6B. The lateral resolution of both detection modes is only determined by the laser intensity distribution at the surface [17] and the SAF-PSF of the bead, shown in Fig. 6D, is nearly identical with the UAF-PSF. Due to the very high collection efficiency of the objective at supercritical angles, the measured SAF intensity of the bead was 1.7-fold higher than the UAF intensity.

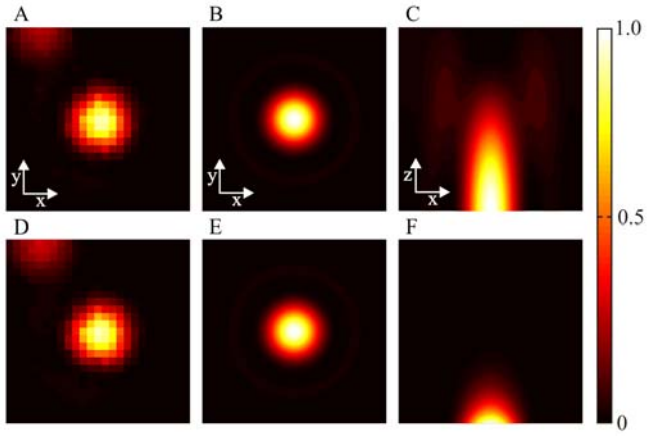

Fig. 6. Normalized point spread functions for UAF collection (upper) and for SAF collection (lower). (A) Scanned UAF image of a 36 nm diameter bead. Pixels: 78 nm × 78 nm. (B) Calculated lateral UAF-PSF at the interface and (C) along z. (D) Scanned SAF image the bead. (E) Calculated lateral SAF-PSF at the interface and (F) along z. Each image has an edge length of 2 μm.

5. Tracking of z-diffusion

The ratio of the simultaneously measured intensities of SAF and UAF can be used to z-localize emitters on the nanometer scale without prior knowledge of the intrinsic brightness

#142685 - $15.00 USD Received 14 Feb 2011; revised 15 Mar 2011; accepted 16 Mar 2011; published 24 Mar 2011

and undistorted by intrinsic intensity fluctuations. Likewise the SAF/UAF ratio is not biased by the emitter's lateral position within the laser focus and can therefore be used to track the z-position of mobile particles. SAF and UAF intensity tracks measured for the diffusion of 36 nm beads through the laser focus are shown in Fig. 7. An aqueous suspension with a low bead concentration was used to minimize the chance to observe more than one bead at a time. The excitation intensity was 1 μW and the cut-off angle of the objective was set to 62°. The photon counts of both detectors were registered with 50 ns temporal resolution (PCI-6602, National Instruments, USA) and binned into intervals of 0.2 ms.

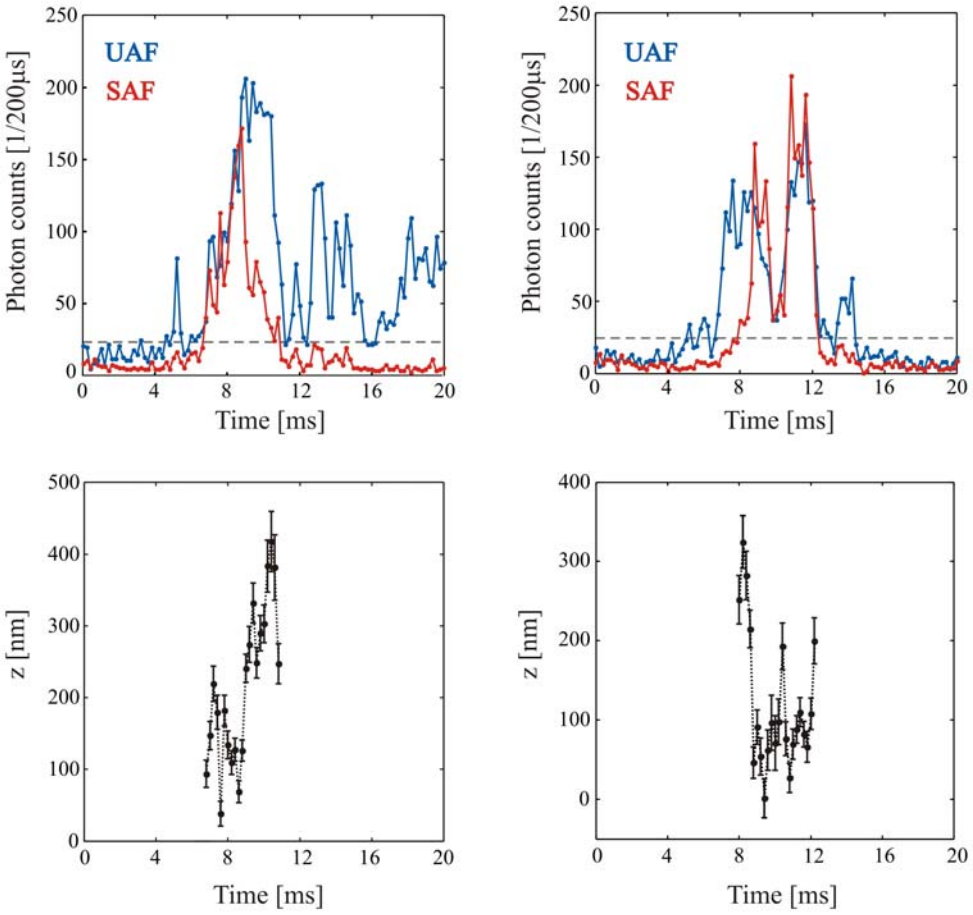

Fig. 7. Diffusion of fluorescent 36 nm diameter beads in water. Top: Raw data of the synchronized SAF and UAF intensities during the transition of two beads (left and right) through the excitation focus. The dashed horizontal line indicates the threshold intensity for the z-localization. Bottom: Z-position of the beads calculated from the data above for every 0.2 ms time bin with SAF and UAF intensities above the threshold.

The synchronized count rates of SAF and UAF exhibited a widely different temporal behavior due to the axial movement of the bead. For beads diffusing at a distance of more than an emission wavelength from the surface the SAF count rate remains on the background level despite the high brightness of the particle measured by UAF. For beads approaching the surface the SAF/UAF ratio approached a value of 1.7. The course of the bead's z-position was calculated for time bins where both intensities exceeded a threshold. Each data point represents a z-value averaged over the binning interval of 0.2 ms. The error bars for the z-

#142685 - $15.00 USD Received 14 Feb 2011; revised 15 Mar 2011; accepted 16 Mar 2011; published 24 Mar 2011

positions were obtained by error propagation for the division of the count rates, governed by shot noise.

6. Single molecule localization

Mouse IgG labeled with the fluorescence dye ATTO 647N (ATTO-TEC, Germany) with a dye/protein ratio of 1.5 was immobilized on a coverslip by non-specific adsorption. Scanned images of the sparsely distributed molecules at the glass/water interface using a circular polarized excitation intensity of 7 µW are shown in Fig. 8. The integration time per pixel was 1.5 ms. The intensity of a molecule in the center of the laser focus was about 100 kHz for SAF and 60 kHz for UAF with a signal-to-background ratio above 20 for both detection modes.

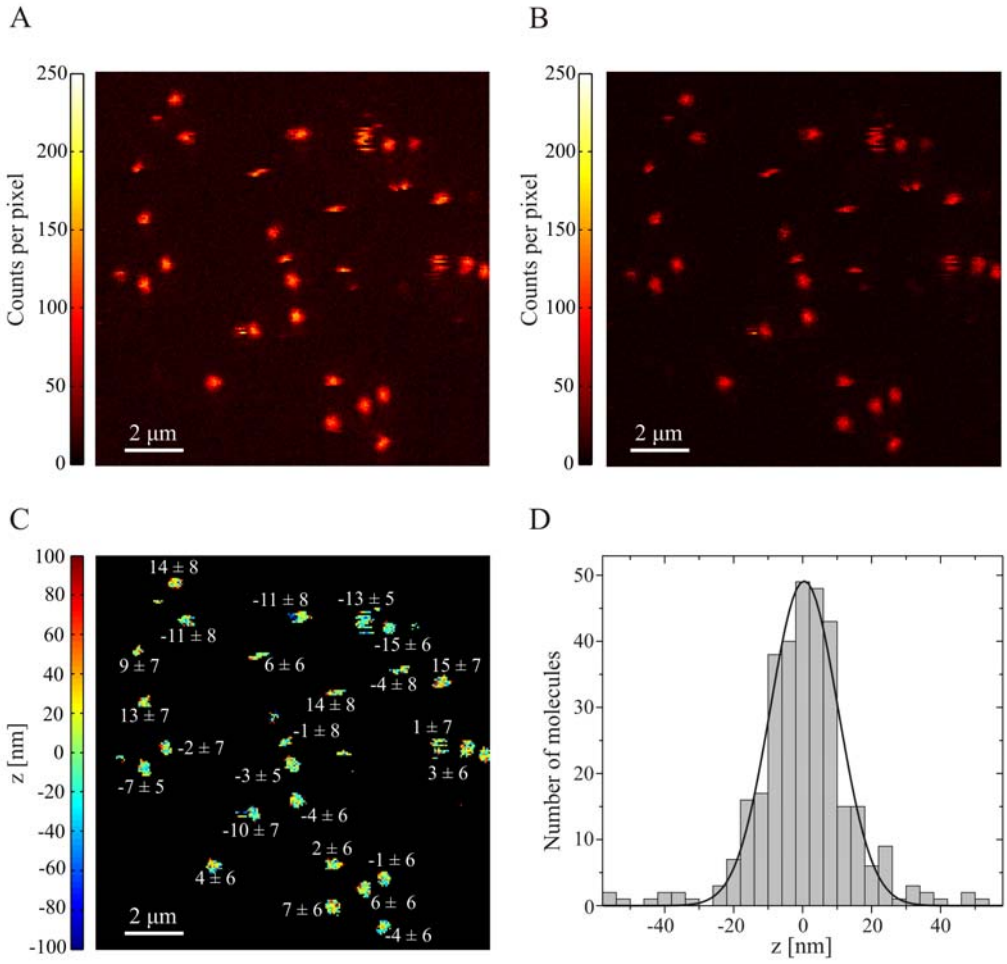

Fig. 8. Single molecule imaging and z-localization of IgG-Atto647N immobilized on a coverslip. (A) SAF image and (B) UAF image of a surface area of 13 µm × 13 µm. (C) Calculated z-positions indicated in nanometers. (D) Z-Localization histogram of molecules found on a larger surface area of 2000 µm^2.

The broadly similar intensity observed for most of the molecules is an indication for the rotation of the fluorophores on the antibodies, faster than the fluorescence lifetime. A fixed orientation of the dipole emitters would result in widely different intensities with dipoles being excited less efficiently the more their absorption dipole moment points out of the surface plane. The free rotation of the dye was confirmed by rescanning the same area with

#142685 - $15.00 USD Received 14 Feb 2011; revised 15 Mar 2011; accepted 16 Mar 2011; published 24 Mar 2011

linear polarized excitation, resulting in virtually identical images of the molecules (data not shown).

The z-localization image shown in Fig. 8C was calculated pixel-wise from the SAF and UAF intensities exceeding a threshold above background. The indicated z-positions of the labeled antibodies were calculated from the mean of their image pixels and the errors were obtained from the standard error of the mean, representing the accuracy of the z-localization for a single scan. For single molecules this error is with 5–8 nm about a factor of three worse than obtained for nanobeads featuring about a ten times higher brightness [17]. Due to Poisson noise the SAF/UAF ratio can be higher than the theoretical value for surface bound emitters. In these cases, the negative z-positions were obtained by linearly extrapolating the z-dependence of the SAF/UAF ratio to negative z-values using the slope at $z = 0$.

Figure 8D shows a histogram generated from a larger number of z-localizations fitted by a Gaussian of 9.7 nm standard deviation, slightly above the localization accuracy. This broadening might be caused by the different positions of the fluorescent labels on the antibodies.

7. Conclusion and outlook

Parallel near-field and far-field microscopy is a powerful approach for measuring topographies and for the study of dynamic processes occurring at interfaces and on membranes. Due to the high collection efficiency of the developed microscope objective, below and above the critical angle, simultaneous single molecule detection with both emission modes has been demonstrated for the first time. The parallel detection volumes open up new perspectives in combination with fluorescence methods based on tight laser focusing, such as fluorescence lifetime imaging microscopy (FLIM), multi-photon excitation (MPE), fluorescence recovery after photobleaching (FRAP), fluorescence correlation spectroscopy (FCS) and stimulated emission depletion (STED). Parallel near-field and far-field detection could be useful in combination with STED to localize emitters with extreme resolution in all three dimensions. Simultaneous FCS above and below the critical angle is a promising approach to discern lateral and axial diffusion components and to measure concentrations at the surface and in solution in parallel.

#142685 - $15.00 USD Received 14 Feb 2011; revised 15 Mar 2011; accepted 16 Mar 2011; published 24 Mar 2011